RESEARCH ARTICLE

Macromolecular Materials and Engineering
www.mame-journal.de

Patterned Electroconductive Networks in Ag-Polyamide 6 Composites by Laser Ablation

Filipa M. Oliveira, Nadya Dencheva, Zlatan Denchev, Filipe S. Silva, Óscar Carvalho, and Caroline G. Moura**

A simple, fast, and cost-effective method to fabricate conductive paths on insulating Ag-containing polyamide 6 (PA6) composites by laser beam treatment is presented in this study. First, Ag-hybrid microparticles (Ag-MP) with a total metal load of up to 19 wt% are synthesized based on a reactive encapsulation strategy utilizing activated anionic polymerization of ϵ-caprolactam in solution, in the presence of Ag nanoparticles. Then, the Ag-MP are compression molded into plates (Ag-PL) on which a scanning laser treatment is applied to create conductive paths in their selected parts. A comparison between structural, morphological, and thermal properties of the Ag-MP and the molded Ag-PL composites is performed. The electric conductive properties of the Ag-loaded hybrid materials are investigated before and after laser ablation, and it is concluded that the laser treatment results in selected paths with widths in the range of 500 µm with conductivity values in the range of 1.12 to 8.90 S m^{-1} while the untreated Ag-PA6 surface remains isolating with conductivity values of 1.27 × 10^{-08} S m^{-1}. These results prove that applying laser ablation with controlled parameters on initially insulating Ag-PL composites can efficiently produce conductive line patterns in composite plates.

1. Introduction

Polymer materials are known for their insulating properties,[1,2] which is a limitation in the development of flexible electroconductive materials. For instance, in a recent work, a bimorph actuator with thermochromic and self-sensing dual functionalities was prepared through an in situ synthesis on a cellulose paper substrate.[3] To overcome this issue, that is, the implementation of polymer matrices in materials with electrical properties, the combination of metals and polymers has been investigated to associate the mechanical and electrical properties of metals with the low density, flexibility, ease of manufacture, and low cost of polymers.[2,4–8] Several studies have demonstrated that the addition of metal particles to polymer matrices improves some properties of the final polymer composite obtained, such as the tensile strength,[9,10] thermal stability,[11–13] and flammability behavior,[11] as well as the optical,[13,14] magnetic,[15–17] electrical,[18,19] and electromagnetic shielding properties.[18,20] Several methods have been used to combine the advantages of metals and polymers in the same material aiming at its application in electric and electronic areas. Methods like physical vapor deposition,[21] chemical vapor deposition,[22] thermal spray metallization,[23] and electroless plating[24] have been used in the development of metal-coated polymer materials. Printing technologies[25,26] are the alternative to fabricate devices based on metal-conductive inks, in which polymer matrices reduce the agglomeration and oxidation of the metal particulate fillers that provide electrical conductivity. It is worth noting that these coating and printing techniques require expensive and specific equipment, high processing costs, and the part sizes and shapes may be subject to limitations. The surface modification of a nonconductor fabric substrate by constructing a polymer-metal-polymer sandwich microstructure coating layer on the surface of a polymer fabric is a low-cost alternative to traditional printing technologies.[27] However, if the substrate is not properly prepared, the adhesion of the metal particles to the substrate can be weak, affecting the metal-substrate interface and therefore their electric conductive properties.

Alternatively, metal particles can be dispersed in a polymer matrix by reactive processing techniques, in which thermoplastic composites are obtained through in situ polymerizations in the presence of the desired payloads. Among the polymerization processes, ring-opening polymerization (ROP) based on an anionic mechanism is the most common approach.[28,29] Thus, considering the processability, chemical, and mechanical resistance of polyamide 6 (PA6),[30] activated anionic ROP (AAROP) of ϵ-caprolactam (ECL) can be applied in the production of PA6 materials. Through reactive microencapsulation of metal loads by AAROP of ECL in a suspension, metal-loaded PA6-based microparticles (MP) were obtained,[31,32] and

F. M. Oliveira, N. Dencheva, Z. Denchev
Institute for Polymers and Composites
University of Minho
Campus de Azurém, Guimarães 4800-058, Portugal
E-mail: denchev@dep.uminho.pt
F. S. Silva, Ó. Carvalho, C. G. Moura
Center of Microelectromechanical Systems
University of Minho
Campus de Azurém, Guimarães 4800-058, Portugal
E-mail: caroline.materiais@gmail.com

The ORCID identification number(s) for the author(s) of this article can be found under https://doi.org/10.1002/mame.202100308

DOI: 10.1002/mame.202100308

combining this novel method with the compression molding (CM) of the MP, metal-containing PA6 composites can be produced.

The PA6-metal molded composites are usually insulators,[32] and to produce conductivity in selected zones, lasers can be used for the surface treatment of those materials. Among the laser processes, laser ablation of polymers presents considerable interest due to its versatility in terms of machining and surface treatment, as well as the possibilities for micro-component fabrication.[33] Furthermore, it is a technique with a lower environmental impact since chemical reagents are not implemented.

Whenever a laser beam interacts with a polymeric surface, several transformations can occur depending on the parameters of the beam such as the laser power, number of pulses, and scanning speed. Increasing the laser energy, vaporization, and ablation of the polymer become well-expressed whereas repeated irradiations in short intervals of time can result in degradation and carbonization that accompany the melting of the polymer matrix.[34] Therefore, the use of controlled laser irradiation for scanning polymers that contain finely dispersed metal loads becomes interesting from both theoretical and applied points of view. In such a way, the polymer that is irradiated by the beam is selectively ablated on the surface, exposing the metal particles that can become sintered. Thus, a conductive network can be possibly created according to the pattern designed by the laser beam.

Some studies on laser ablation of neat polyamides can be found in the literature,[34–36] however, polyamide-metal composites with electrical conductivity in customized areas by a selective scanning laser treatment have yet to be reported. Here, we report the first results on the synthesis of Ag-loaded PA6 MP (Ag-MP) through AAROP in solution and their transformation into PA6 composite plates (Ag-PL) by CM. Thermal methods, electron microscopy, and X-ray scattering were used to characterize the Ag-MP and Ag-PL samples. Then, an Nd: YAG laser was used to irradiate the Ag-PL samples exposing the Ag particles in selected paths, and conductivity measurements were performed after various laser treatments of the Ag-PL samples. Ultimately, conclusions about possible applications of the Ag-PA6 hybrid materials produced were presented.

2. Experimental Section

2.1. Materials

The ECL monomer with reduced moisture content for AAROP (AP-Nylon caprolactam) was delivered from Brüggemann Chemical, Germany. As polymerization activator, Brüggolen C20 from Brüggemann Chemical, Germany (C20) was used. According to the manufacturer, it contains 80 wt% of blocked di-isocyanate in ECL. The initiator sodium dicaprolactamato-bis-(2-methoxyethoxo)-aluminate (Dilactamate, DL) was purchased from Katchem, Czech Republic, and used without further treatment. Powdered Ag (≥99% pure, with an average grain size of 230 nm) was supplied by Metalor Technologies, USA. Toluene, xylene, methanol, and other solvents, all "puriss" grade, were purchased from Sigma Aldrich and were used as received.

Table 1. PA6 MP—sample designations, reaction yields, and sample composition.

Sample designation	Load [wt%][a]	Composition [vol%][b]		MP yield [wt%][c]	Real load, *RL* [wt%][d]
		Metal	PA6		
PA6	-	0.00	100	56.0	-
PA6/Ag10	10	2.40	97.6	48.2	18.6

[a] In respect to the weight of ECL in the starting polymerization medium; [b] Represents the relation between the volumes of metal and PA6 in the respective sample; [c] In respect to the sum of the ECL and Ag particles weight; [d] Determined by TGA according to Equation (3).

2.2. Sample Preparation

Ag-MP were produced by solution-precipitation AAROP of ECL according to the procedure described in detail previously.[31,32] The metal payload was used without any physical pretreatment or chemical functionalization. Typically, about 0.5 mol of ECL and the desired amount of Ag powder (10 wt% in respect to ECL) were added to 100 mL of 1:1 toluene/xylene mixture while stirring, under a nitrogen atmosphere, refluxing the reaction mixture for 10–15 min. Subsequently, 3 mol% of DL and 1.5 mol% of C20 were added at once. The reaction time was always 2 h from the moment of catalytic system addition, maintaining the temperature in the 125–135 °C range at a constant stirring of ≈800 rpm. The Ag-MP that formed as a fine powder were separated from the reaction mixture by hot vacuum filtration, washed several times with methanol, and dried for 30 min at 80 °C in a vacuum oven. Neat empty PA6 MP were prepared analogously, without adding metal particles.

By conventional CM of the MP synthesized, molded plates were prepared in a 25-ton hydraulic hot press (Moore, England) using a rectangular mold with dimensions 70 mm × 70 mm × 2 mm, pressing for 8 min at 230 °C at a pressure of ≈3–4 MPa. **Table 1** presents the sample designations and the respective compositions.

Specimens with 10 mm width were cut from the CM plates for the laser treatment experiments. The experimental setup for ablation of a polymer superficial layer and exposure of the enclosed Ag particles included the use of a pulsed Nd: YAG laser with a wavelength of 1064 nm, frequency of 20 Hz, a pulse width of 35 ns, and a spot diameter of 3 μm. Three laser scanning parameters were varied in this study, namely the laser power (P) which represents the laser beam energy delivered per pulse in Watts (W), the scanning speed (v) at the leading edge of the beam front in mm s^{-1}, and the number of scans (n) carried out by the laser during the process, evaluating their influence on the electrical properties of the Ag-PL composites. The laser energy density E, can be calculated from those parameters according to Equation (1):

$$E = \frac{P \cdot n}{v}, \text{J mm}^{-1} \quad (1)$$

Table 2 shows the parameters of the laser beam treatment used in this study. **Figure 1** shows a schematic representation of all the steps related to the sample preparation.

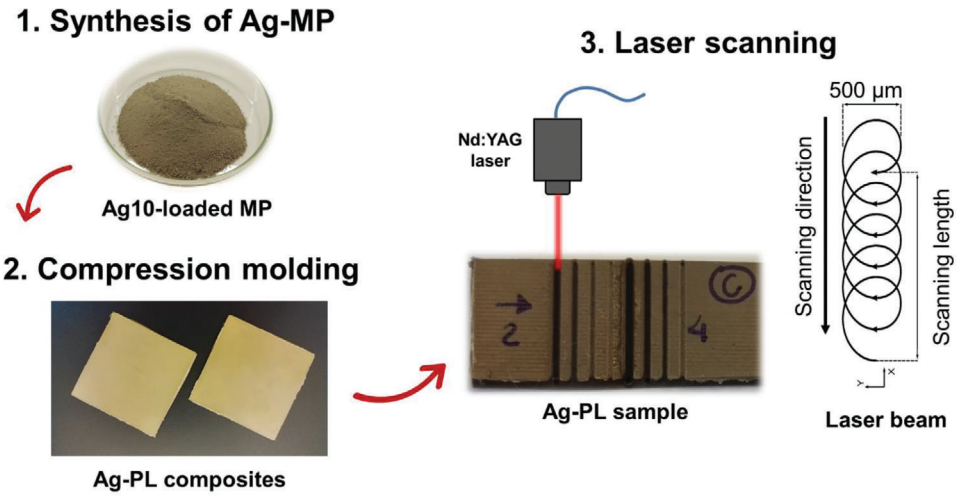

Figure 1. Illustration of the main experimental steps for the samples preparation: 1) visual aspect of the Ag-MP; 2) visual aspect of Ag-PL composites prepared by compression molding of the respective Ag-MP; 3) visual aspect of a Ag-PL sample after applying the laser scanning treatment with the illustration of the laser beam movement.

Table 2. Basic parameters of laser beam treatment and their impact on the electrical conductivity after it in the Ag-PL samples. The electrical conductivity of the samples before the treatment was 1.27×10^{-08} S m^{-1}. Reproduced with permission.[32] Copyright 2016, J. Mater. Sci.

Condition[a)]	Power [%]	Power [W]	n[b)]	Scanning speed [mm s^{-1}]	Energy density[c)] [J mm^{-2}]	Electrical conductivity [S m^{-1}]
A	100	6.0	4	2	12.0	8.04 ± 0.25
				4	6.00	7.54 ± 0.16
				8	3.00	4.61 ± 0.15
				16	1.50	4.34 ± 0.85
			2	2	6.00	8.08 ± 0.24
				4	3.00	5.16 ± 0.74
				8	1.50	3.60 ± 0.11
				16	0.75	1.87 ± 0.74
B	25	1.5	4	2	3.00	7.94 ± 0.33
				4	1.50	8.90 ± 0.28
				8	0.75	3.31 ± 0.13
				16	0.38	5.01 ± 0.27
			2	2	1.50	8.13 ± 0.78
				4	0.75	2.43 ± 0.74
				8	0.38	1.12 ± 0.36
				16	0.19	3.90 ± 0.43

[a)] Value determined based on the experimental procedure in ref. [32]; [b)] n = number of laser scans (see Equation (1)); [c)] Calculated according to Equation (1).

2.3. Methods

Scanning electron microscopy (SEM) studies were performed in a NanoSEM-200 apparatus of FEI Nova (USA) using mixed secondary electron/back-scattered electron in-lens detection. The MP and PL samples were observed after sputter-coating with Au/Pd alloy in a 208 HR equipment of Cressington Scientific Instruments (UK) with high-resolution thickness control.

The average viscometric molecular weight, M_v, of the empty MP was determined by intrinsic viscosity measurements in 97% sulfuric acid at a concentration of 0.2 g dL^{-1} with a suspended level Ubbelohde viscometer thermostatted at 25 °C. Using the Mark–Houwink equation with $K = 5.066 \times 10^{-4}$ and $\alpha = 0.74$ for PA6[37], the M_v values were determined. Flow times were recorded as an average of five runs.

Differential scanning calorimetry (DSC) measurements were carried out in a 200 F3 equipment of Netzsch (Germany) at a heating rate of 10 °C min^{-1} under a nitrogen purge. The typical sample weights were in the 10–15 mg range. The degree of crystallinity, X_c, of the PA6 matrix was calculated according to Equation (2):

$$X_c = \frac{\Delta H_m^i}{w \cdot \Delta H_m^0}, \% \quad (2)$$

where ΔH_m^i is the registered melting enthalpy of the current sample, w is the weight fraction of the polymer present in the sample, and ΔH_m^0 is the melting enthalpy of a 100% crystalline PA6 (190 J g^{-1}).[38]

The effective inorganic load, RL, in MP and PL samples was determined using thermogravimetric analysis (TGA) in a Q500 gravimetric balance (TA Instruments, USA) heating the samples to 600 °C at 10 °C min^{-1} in a nitrogen atmosphere. The RL was calculated according to Equation (3):

$$RL = R_i - R_{PA6}, \% \quad (3)$$

where R_{PA6} is the carbonized residue at 600 °C of empty MP and R_i represents the carbonized residue of the respective loaded MP measured by TGA.

X-ray diffraction (XRD) patterns of Ag-PL samples were acquired at room temperature with a step time of 1 s and step size of 0.02° min^{-1} using a Bruker AXS D8 Discover (Bruker, USA) diffractometer in Bragg–Brentano geometry applying Cu-Kα radiation with wavelength $\lambda = 1.54060$ Å.

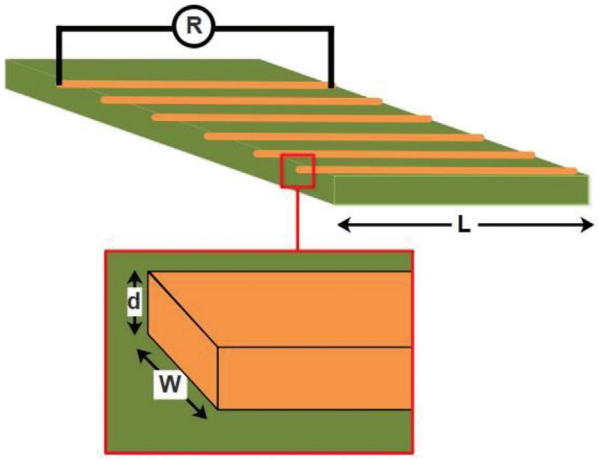

Figure 2. Schematics of the parameters included in the electrical characterization of the PA6/Ag10 molded samples after the laser scanning treatment (see also Equation (4)).

Resistivity measurements were performed using a Fluke 8846A 6.5 Digit Precision Multimeter (Fluke Europe B.V., The Netherlands). A two-probe test was used, with 10 mm between the measuring probe points. Electrical resistivity, ρ, was determined following Equation (4):

$$\rho = R \cdot \frac{W \cdot d}{L},\ \Omega\times\mathrm{m} \tag{4}$$

where R is the electrical resistance, and L, W, and d are the parameters of the laser beam, that is, length, width, and depth, respectively. Then, electrical conductivity, σ, was calculated as the reciprocal value of the electrical resistivity obtained:

$$\sigma = \frac{1}{\rho},\ \mathrm{S\ m^{-1}} \tag{5}$$

For each laser condition, three samples were prepared, and each sample was measured three times, taking the arithmetical mean as a final value of conductivity. A simple configuration of the electrical characterization is shown in **Figure 2**.

3. Results and Discussion

3.1. Synthesis of Neat and Loaded PA6 Microparticles

The mechanism related to the formation of empty PA6 MP was postulated by Oprea and Dan[39,40] and Rico et al.,[41] and more recently proved in the presence of different payloads including metals.[31] Hence, if the Ag nanosized particles are dispersed in the constantly stirred reaction medium, as the AAROP progresses, they become entrapped into the viscous droplets formed by growing PA6 polymer molecules and nucleate the PA6 crystallization to MP. The same process, but as a result of homo nucleation, occurs in the absence of metal payload.

Table 1 shows that the real load of Ag in the hybrid MP is close to 19 wt%, that is, almost two times higher than the content of metal introduced in the reaction medium in respect to the ECL monomer before AAROP. This observation is explained by the polymerization yield of the Ag-MP that is slightly below 50%. At the same time, the neat PA6 MP displays a degree of conversion to the polymer of 56%. This means that the presence of Ag nanoparticles does not hinder or block the anionic polymerization process.

The M_v of the empty PA6 MP was found to be 33 100 g mol^{-1}, which was by 10–15% lower than the values of commercial hydrolytic PA6 brands, as M_v was measured at the same conditions. The M_v of the hybrid Ag-containing MP cannot be determined correctly due to the chemical reaction between the metal and the sulfuric acid leading to carbonization and precipitation of the polymer solution. However, it is expected that the molecular weight of the Ag-loaded MP is similar to that of the empty MP since the Ag particles do not seem to affect the AAROP mechanism and the ECL conversion significantly.

3.2. Scanning Electron Microscopy Studies of Microparticles

Figure 3 presents information about the Ag-loaded MP as compared to the empty MP. The latter (Figure 3a,b) are present in the form of aggregates of partially fused PA6 spheroids with typical diameters of 5–10 µm that form the final particles with average diameters of 20–30 µm, which is close to previously reported data.[31] Figure 3b shows that the empty MP are porous, with a scaffold-like morphology, the pore sizes varying in the 250–500 nm range. The irregular spherical shape of Ag particles is observed in micrographs Figure 3c,d, with sizes of about 70–300 nm. As seen from Figure 3e,f, the morphology of the Ag-containing MP is rather similar to that of the empty MP, maintaining a porous and scaffold-like topography with average pore diameters below 500 nm.

3.3. TGA Properties

Empty and Ag-containing MP, as well as the respective compression-molded plates, were analyzed by TGA to compare the *RL* values and to assess the influence of the metal particles on the thermal stability of the Ag-loaded materials produced. **Figure 4** displays the weight retention TGA curves and Table S1, Supporting Information summarizes the numerical data of the thermal degradation derived from them.

As expected, the *RL* in the PA6 MP and the respective molded plate are virtually the same (Table S1, Supporting Information). The Ag-PA6 MP (Figure 4a) and the respective molded plate (Figure 4c) display almost identical thermal stability as compared to the neat PA6 samples. In the empty MP, the temperature of initial degradation T_{in} = 302.5 °C, and the maximum degradation temperature is reached at T_{max} = 339.3 °C. With the incorporation of Ag filler, T_{in} = 306.7 °C and T_{max} = 335.8 °C. Moreover, in the Ag PL, there are two peaks in their differential TG curves (Figure 4d; Table S1, Supporting Information) at T_{max} = 350.3 and 373.8 °C. This could be related to two degradation events of the PA6 phase at the Ag-polymer interface and PA6 away from the metal particles, the volume of both PA6 fractions being similar. Generally, an easier dissipation of the heat by the well-dispersed Ag filler particles can be supposed to delay the degradation of

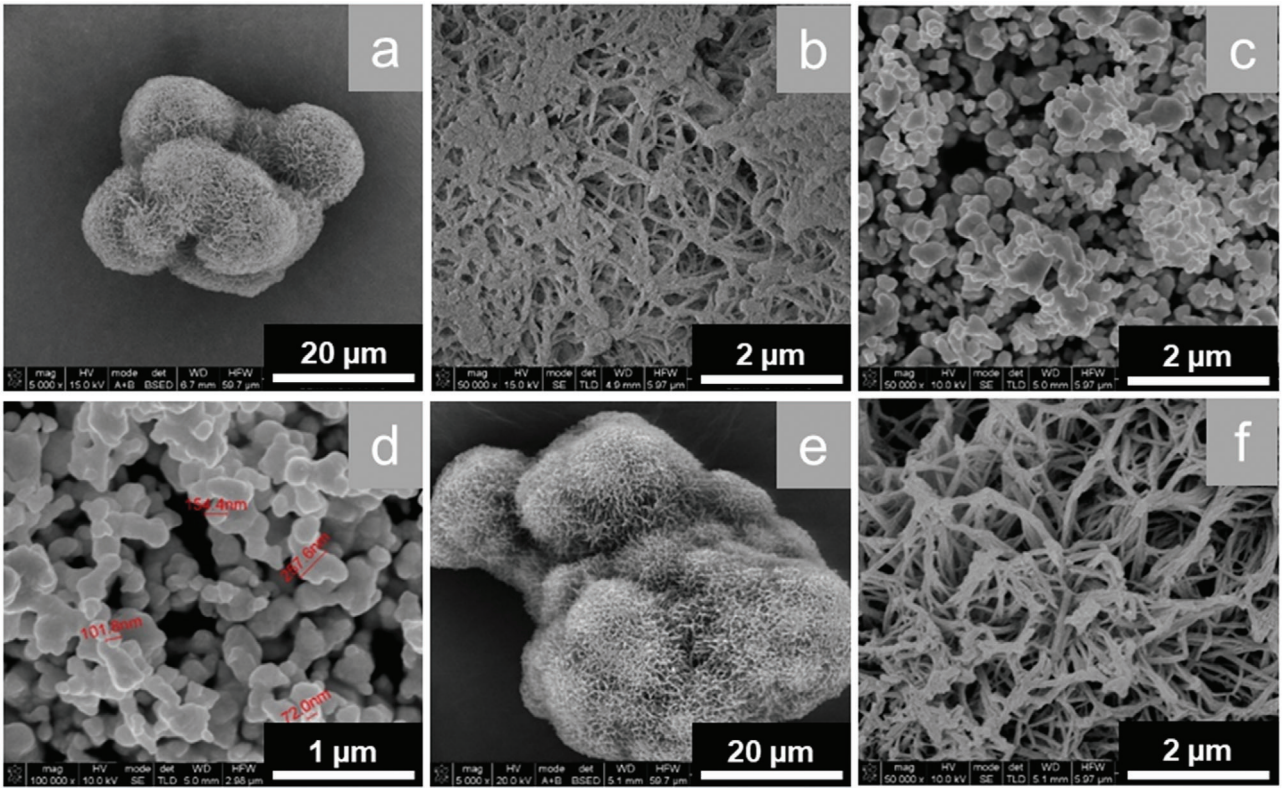

Figure 3. Selected SEM micrographs of: a,b) empty MP; c,d) neat Ag particles; e,f) Ag-loaded MP.

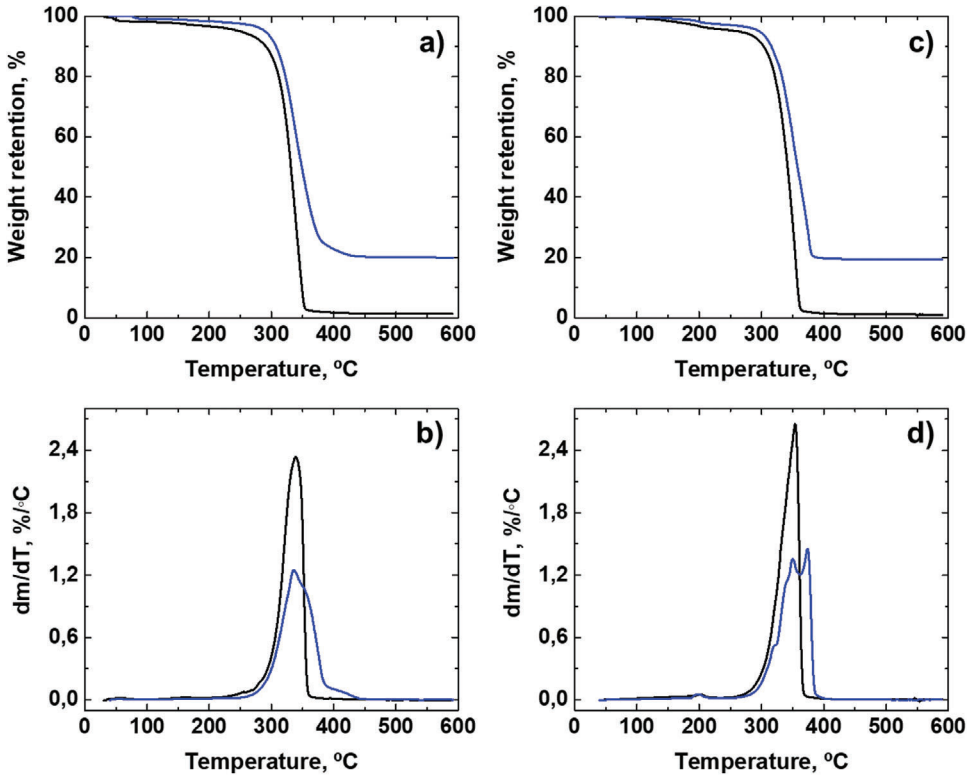

Figure 4. Weight retention as a function of temperature and respective integral curves of a,b) MP and respective c,d) compression-molded samples in N_2 atmosphere. Black lines—neat PA6; blue lines—PA6/Ag10.

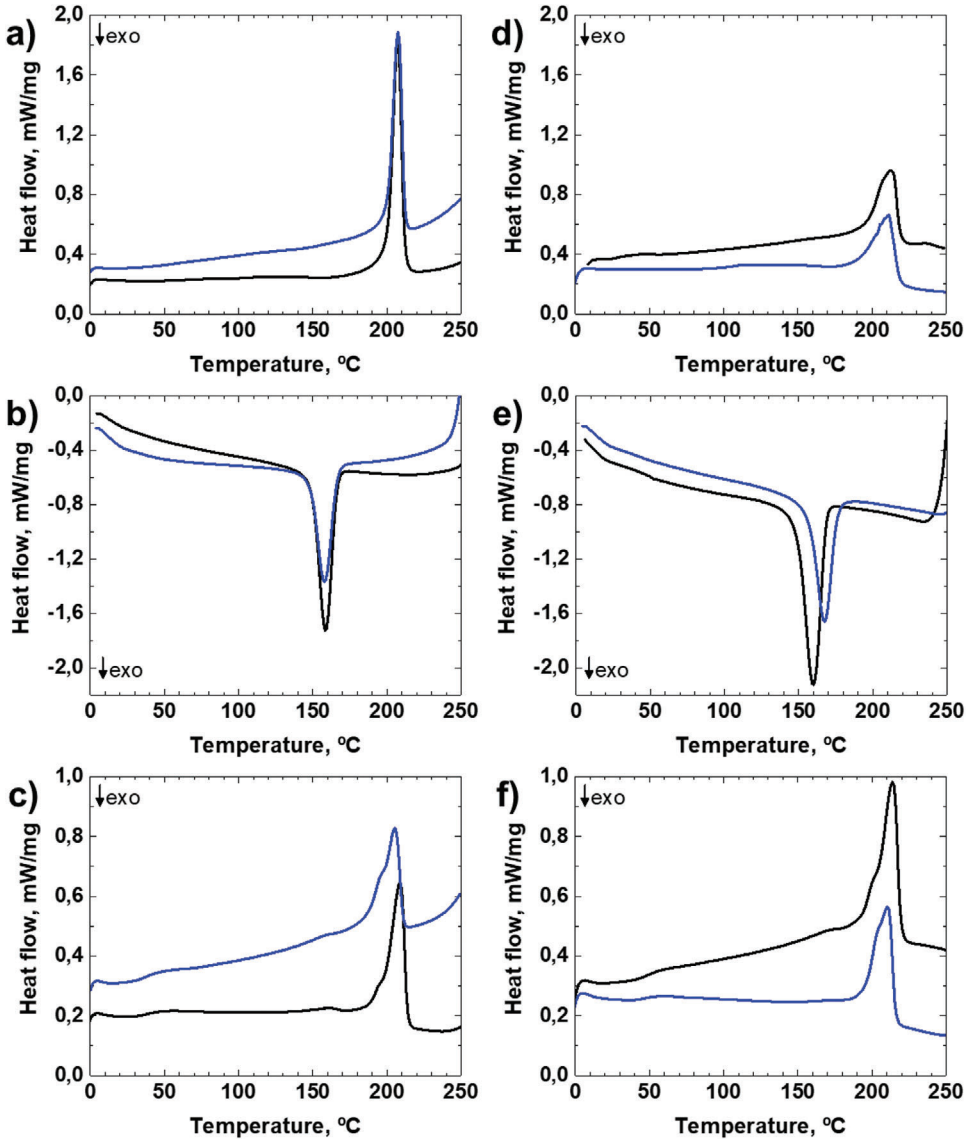

Figure 5. DSC traces of a–c) MP samples and d–f) respective compression molded plates. Top images: first DSC scans; middle images: recrystallization from the melt; down images: second DSC scans. Black lines—neat PA6; blue lines—PA6/Ag10.

the composite as compared to the neat PA6 molded plate. Therefore, in terms of heat resistance, the presence of Ag filler particles slightly improves the thermal degradation of the PA6 matrix in either particulate or molded hybrid materials. This is important since the Ag-containing molded plates will be ablated by laser scanning.

3.4. DSC Properties

For a better evaluation of the effect of Ag filler on the thermal behavior of the PA6 matrix, DSC analyses were performed measuring the melting temperature T_m, crystallization temperature T_c, and glass transition temperature T_g, as well as the degree of crystallinity, X_c^{DSC}. **Figure 5** displays the DSC traces of the MP samples and the respective compression-molded plates during the first heating scan, recrystallization, and second heating scan. All data extracted from the DSC curves are presented in Table S2, Supporting Information.

The two MP samples display a single melting peak (Figure 5a) in the first heating scan. The Ag-containing MP shows a melting temperature at $T_m = 207.6$ °C (Table S2, Supporting Information), and for the neat PA6 MP $T_m = 207.3$ °C, that is, the T_m in MP samples is not affected by the presence of the Ag filler. Crystallization from the melt of the neat and Ag-containing MP samples (Figure 5b; Table S2, Supporting Information), displays almost coinciding single crystallization peaks at 158.6 and 157.9 °C, respectively. Comparing the first (Figure 5a) and the second heating (Figure 5c) scans of the MP samples, it can be seen that the main melting peaks are similar remaining between 205 and 209 °C. However, both endotherms during the second heating scan become broader, less intense, and with a low-temperature

shoulder. This observation suggests the increased presence of the lower melting point γ-PA6 polymorph in the recrystallized samples, coexisting with the predominant α-PA6 phase found at a higher temperature.[42]

The DSC traces of the compression-molded plates are shown in Figure 5d–f, Table S2, Supporting Information. They are analogous to the DSC traces of the second scan of MP samples which is expected since the molded plates were prepared by CM of the respective MP. The broader peaks on the first heating scan (Figure 5d) indicate the coexistence of the α- and γ-PA6 polymorphs.[42,43] Concerning the X_c^{DSC} values (Table S2, Supporting Information), the presence of Ag filler induces up to 4% increase as compared to the neat PA6 samples—either MP or molded plates.

The data in Table S2, Supporting Information allow a comparison between the T_g of the empty and loaded MP obtained during the 2nd heating scan. The T_g values of the empty and Ag-containing MP are similar, both close to 39 °C, the difference being in the margin of the experimental error. After the CM process, both molded samples show higher T_g values in the range of 47–48 °C, the difference to the MP samples reaching 9 °C. This indicates that in the powder-like MP samples the segmental mobility of the macromolecules in the amorphous domains is higher than in the respective molded plates. Most probably, this effect can be related to the CM process producing denser microstructures due to the pressure applied during the transformation of the MP into molded composites.

3.5. Scanning Electron Microscopy Studies of Composites after Laser Treatment

In order to interpret and understand the effect of the selected laser scanning conditions on the Ag-PL composites produced by CM, SEM analyses were performed. It must be pointed out that neat PA6 molded plates were not analyzed by SEM since they were highly sensitive to laser machining parameters. The low melting and thermal degradation temperatures, as well as the low thermal diffusivity of PA6, did not allow laser machining of this sample due to its fast degradation. Therefore, only Ag-PL samples were investigated after the laser scanning treatment. Selected SEM micrographs of the laser paths on the Ag-PL samples with different conditions are shown in **Figure 6** a, b, c, d and Figures S1–S3, Supporting Information. For each condition, the scanning speed evolution ($v = 2$ to 16 mm s^{-1}) and energy density (0.38 to 12 mm^2) are indicated.

As can be observed (Figure 6 a, b, c, d; Figures S1–S3, Supporting Information), the Ag nanoparticles are well dispersed in the polymer matrix in all conditions. The homogenization of the metal particles within the PA6 matrix is well visible in micrographs a1–d1 (cross-view) for each condition, confirming that the solution/precipitation AAROP in the presence of Ag filler is a useful route for the preparation of Ag-containing composites.

Another general conclusion from the SEM study of all samples is that removal of the superficial polymer layer by laser ablation was achieved. In general, increasing the n values from 2 (Figure 6 a-d; Figure S1, Supporting Information) to 4 passes (Figures S2,S3, Supporting Information) makes the removal of the surface polymer layer more effective, which leads to an increase of the Ag particles exposure. For all the conditions, the width of the path increased with increasing the energy density, because of the heat-affected zone that becomes more pronounced at higher energy densities.

Further, it should be noted that the absorption characteristics of polymers depend on their structure, but it is strongly influenced by the presence of loads or additives.[44] In this case, when the laser beam is directed onto the surface, the radiation is absorbed by the metal particles that are dispersed in the polymer matrix. At the same time, the influence of the processing parameters and their effects on the polymer irradiated by Nd: YAG laser source is complex and it depends on the multiple parameters associated with the nature of the polymer.[45] The energy provided by the laser beam induces the heating of the material, reaching melting or even vaporization temperatures. This way, the topmost layer of polymer is removed, and the surface topography is modified, as observed in micrographs a1–d1 and a2–d2 of Figure 6 and Figures S1–S3, Supporting Information.

The laser power also influences metal particle exposure. From condition A ($P = 6$ W, Figure 6; Figure S2, Supporting Information) to condition B ($P = 1.5$ W; Figures S1,S3, Supporting Information), the ablation rate was higher as well as the depth of the laser paths. In micrographs a1–d1 of Figure 6 and Figures S1–S3, Supporting Information, the effect of laser power on path depth is visible.

By analyzing the number of passes, the ablation of the polymer matrix was more distinguishable when $n = 4$ (Figure 6; Figure S2, Supporting Information). On the one hand, Ag filler particles become more exposed (micrographs a3–d3 of Figure 6; Figure S2, Supporting Information), however, this effect can compromise the aesthetic aspects. On the other hand, if $n = 2$(Figures S1,S3, Supporting Information) a significant difference is observed in the appearance of the composites since the ablation of the polymer layers is less destructive. Although fewer Ag particles are exposed (micrographs a3–d3 of Figures S1,S3, Supporting Information), the visual appearance of the specimens was improved, which can be important for some potential applications.

The scanning speed was the most influential parameter in the results obtained with the laser scanning experiments performed. According to micrographs a1–d1 and a2–d2 of Figure 6 and Figures S1–S3, Supporting Information, the paths become more pronounced at lower scanning speeds. Thus, a higher polymer ablation was achieved, as a consequence of the highest energy densities and laser irradiation time on the sample. Thereby, Ag particles were more exposed, as verified from micrographs a3–d3 of Figure 6 and Figures S1–S3, Supporting Information. Again, aesthetic aspects should be considered, since at lower scanning speeds there is a higher deterioration of the specimens by the laser beam.

The combination of the effects of lower scanning speeds (2 and 4 mm s^{-1}) with lower laser power (1.5 W) resulted in a superior polymer ablation and metal particle exposure without compromises to the aesthetic aspects of the sample (micrographs a,b of Figures S1,S3, Supporting Information). However, from $v = 8$ to $v = 16$ mm s^{-1}, at the same laser power of 1.5 W, less polymer was removed (micrographs c,d of Figures S1,S3, Supporting Information), as a consequence of the lesser laser irradiation time on the specimen surface. In this case,

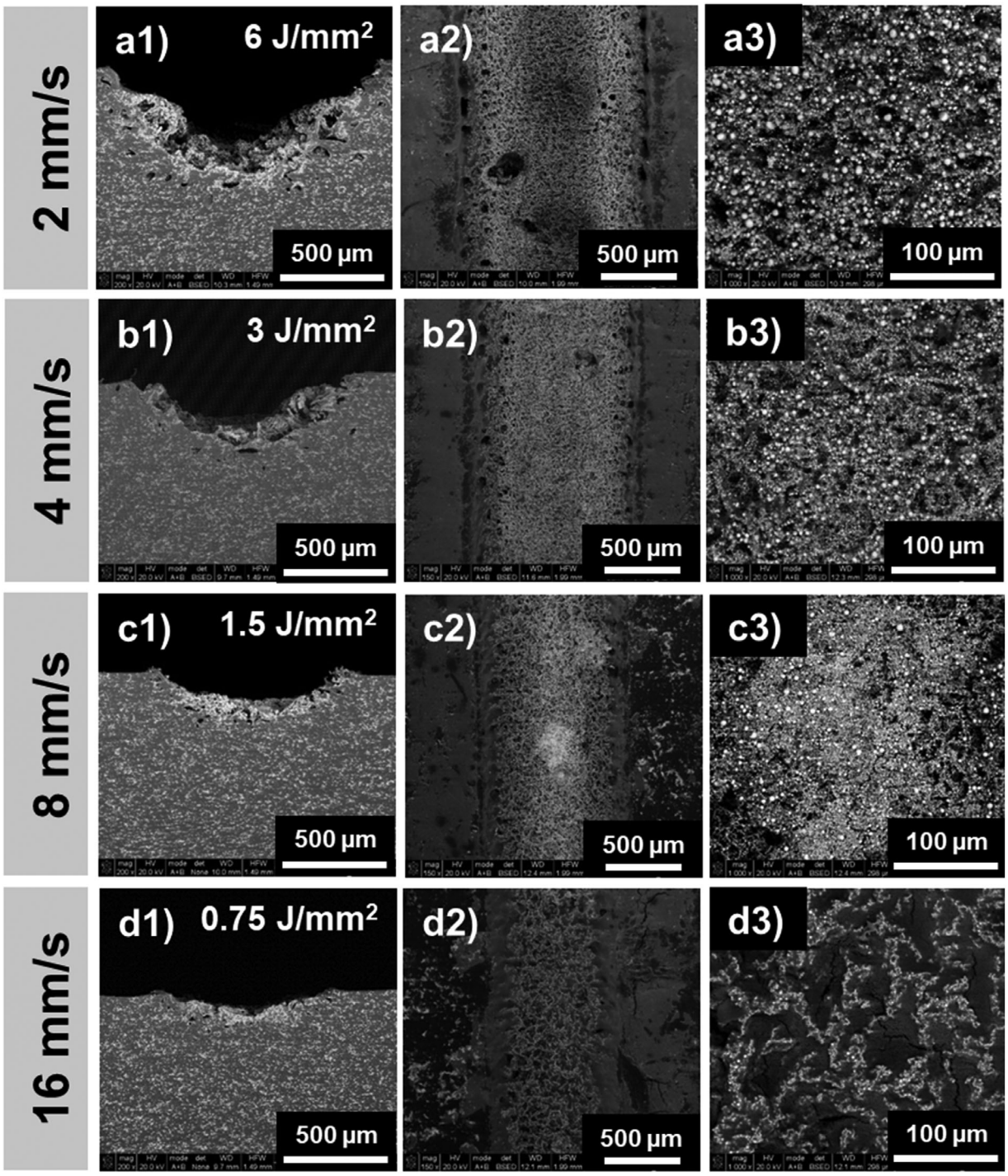

Figure 6. Selected SEM micrographs of Ag-PL composite after laser scanning treatment by using condition A (6 W laser power) with $n = 2$. Left (a1, b1, c1 and d1): cross section view; center (a2, b2, c2 and d2) : top view; right (a3, b3, c3 and d3): magnification of the top view.

fewer Ag particles are exposed, which can negatively affect the electrical conductivity since metal particle exposure is reduced (micrographs c,d of Figures S1,S3, Supporting Information). In contrast, higher laser power (6 W) combined with less scanning speeds (micrographs a,b of Figure 6; Figure S2, Supporting Information) results in critical polymer degradation.

Considering all the laser scanning parameters and their effects as described above, it is evident that further studies on the laser setup optimization can be made keeping in mind the potential of these molded composites in electronic applications.

Other aspects can be also observed in the SEM micrographs such as the size of the Ag filler particles after the laser

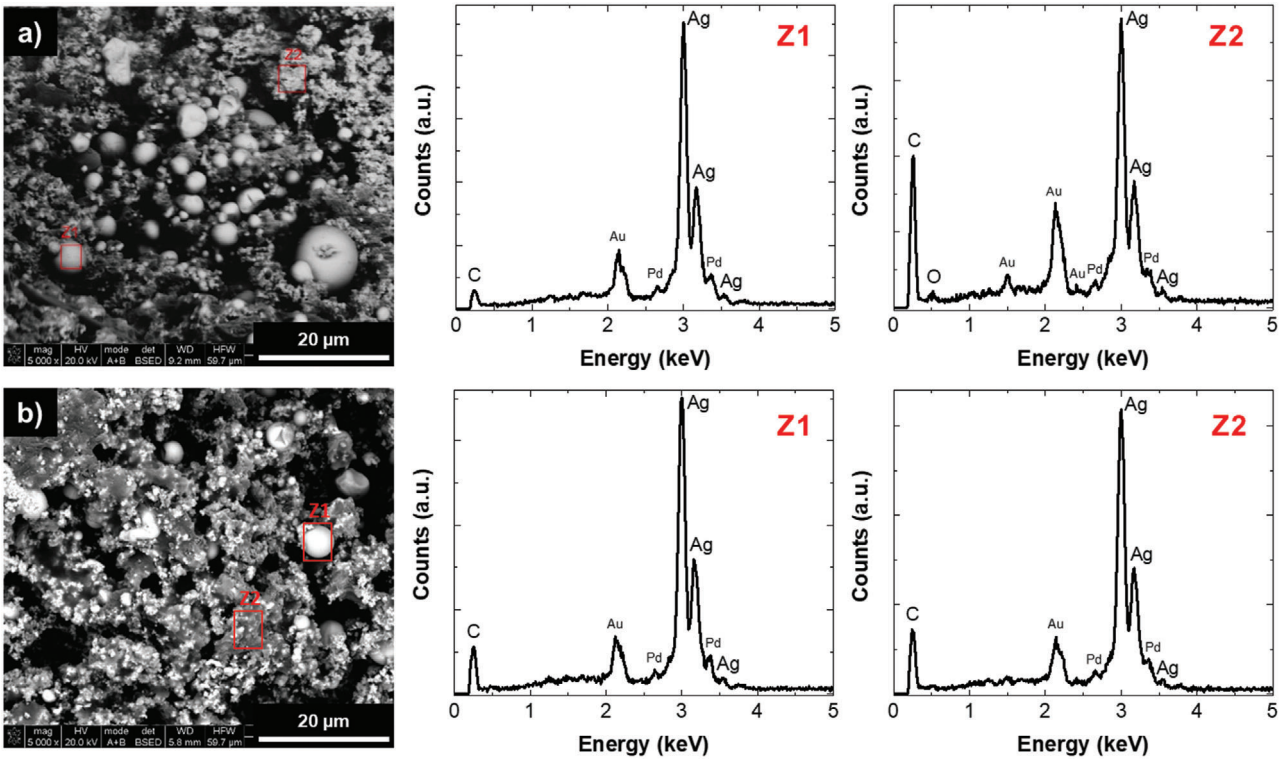

Figure 7. Micrographs (on the left) of EDS analysis on Ag-PL samples exposed to laser treatment with $P = 6$ W and $v = 2$ mm s^{-1}, varying the number of scans: a) $n = 4$, b) $n = 2$, and respective EDS spectra (on the right) in the Z_i sites.

scanning treatment. A considerable increase of the size after the laser scanning treatment is observed at higher energy densities (micrographs a3–b3, Figure 6; Figures S1–S3, Supporting Information), because of the thermal effects of the laser beam. Bearing in mind that the processes of diffusion of particles are activated by temperature,[46] the results obtained indicate that there is a movement of Ag particles during the laser treatment. This means that the temperature increase causes the Ag particles motion and a consequent contact between them, which leads to their coalescence, and then larger spherical aggregates are formed.

Then, the specimens exposed to the most energetic laser scanning conditions ($P = 6$ W, $v = 2$ mm s^{-1}, and $n = 2$ or 4) were analyzed by energy-dispersive X-ray spectroscopy (EDS) to evaluate the effects of the laser treatment on the oxidation and carbonization states of the elements in the Ag-PL samples. The results are summarized in **Figure 7** and Table S3, Supporting Information. On the site Z1 (Figure 7; Table S3, Supporting Information), in addition to the expected Ag composition, carbon (C) was identified. The C registered (between 4 and 10 wt%) can be due to the thermal degradation of the polymer matrix, being higher in the condition $n = 4$ (9.67 wt%) where the energy density is higher. In site Z2 (Figure 7; Table S3, Supporting Information), along with Ag and C, oxygen (O) was identified. Bearing in mind the carbonyl groups in the PA6 molecular chains, it is suggested that the detected O belongs to the polymer matrix. Furthermore, in the analyzed areas (Z2 in Figure 7), it is visible that the laser beam did not completely remove the polymer layers, contributing to the presence of O and C.

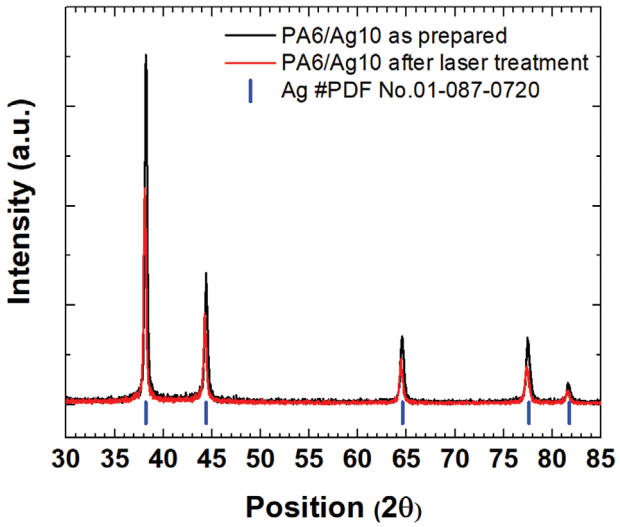

Figure 8. XRD patterns of PA6/Ag10 sample before and after laser scanning treatment (at $P = 6$ W, $n = 4$). Diffraction peaks are compared with the powder diffraction file (PDF) of Ag particles detailed in PDF No. 01-087-0720.

In addition, XRD analyses were performed (**Figure 8**; Table S4, Supporting Information) with the samples exposed to the most severe laser scanning conditions ($P = 6$ W, $v = 2$ mm s^{-1}, and $n = 4$). As can be seen from the diffraction patterns obtained (Figure 8), the crystalline phase of the Ag was not affected by the laser

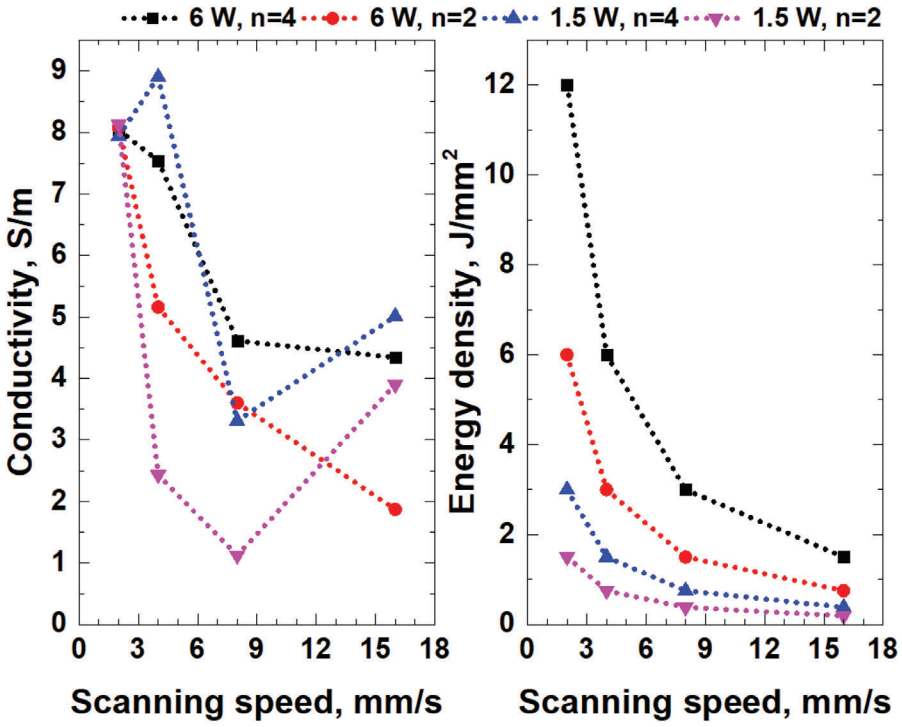

Figure 9. a) Electrical conductivity and b) energy density as a function of laser scanning speed.

treatment applied to it, which is consistent with the crystalline structure of Ag particles detailed in the powder diffraction file (PDF) PDF No.01-087-0720.[47] Since silver oxide is not detected, it can be suggested that the high temperature resulting from the laser beam during the surface treatment may cause the decomposition of possibly formed silver oxide particles.

3.6. Electrical Conductivity

The electrical conductivity (σ) was determined for all laser treatment conditions applied on the Ag-PL samples using Equations (4) and (5). Numerical data are summarized in Table 2 and **Figure 9** displays the plots of σ (Figure 9a) and energy density (Figure 9b) as a function of the laser scanning speed.

As attested in the previous study on PA6-metal hybrids obtained via microencapsulation,[32] those systems maintain the electrical insulating properties of the neat PA6 matrix (in the range of 10^{-10} to 10^{-9} S m^{-1} even if it is used a metal concentration up to by 30 wt%. The Maxwell–Wagner–Sillars interfacial polarization theory predicts no electrical conduction in a composite material containing conductive filler particles dispersed in an insulating matrix at any filler volume fraction.[48] The metal particles are always enclosed by the insulating matrix, blocking the free movement of charges to achieve a conductive network.

In this work, by applying a laser treatment, the polymer matrix was removed in selected paths, exposing the Ag particles as seen from the SEM studies in Figure 6 and Figures S1–S3, Supporting Information. For the laser scanning conditions studied, σ values in the range of 1.12 to 8.90 S m^{-1} were measured, meaning that the Ag particles promote carrier mobility on the ablated surface. The conductivity of bulk silver is 6.80×10^7 S m^{-1}, meanwhile semiconductors like pure germanium and silicon exhibit values of, respectively, 1.67 and 4.35×10^{-4} S m^{-1}.[49] Thus, it can be assumed that the laser treatment applied in this investigation allowed obtaining thermoplastic composites with semi-conductive properties. Further, as a consequence of the coalescence mechanism and thus the contact between Ag particles, the resulting carrier flux leads to the formation of a conductive network, providing an improvement of the electrically conductive properties of the Ag-PL molded composites. All this is in good agreement with earlier studies stating that by increasing the particle size of the metal load, larger contact areas are created, enhancing electrical properties.[50]

As seen from Table 2 and Figure S3a, Supporting Information, for all the scanning laser conditions studied, the increase of the scanning speed leads to a slight decrease in the σ values. The laser ablation rate is lower, and the energy density provided (Figure S3b, Supporting Information) is not enough to remove the insulating polymer that encloses the Ag particles. This event is more visible at high scanning speed (16 mm s^{-1}), in specific when the energy density is lower than 1.5 J mm^{-2} (micrographs d3) of Figure 6 and Figures S1,S3, Supporting Information. Although at lower scanning speeds less polymer was removed in the paths irradiated by the laser beam, a conductive network was built through the Ag particles as confirmed by the σ values obtained (Table 2). This fact suggests that at lower energy densities a suitable compromise can be found between the laser scanning setup and the aesthetic aspects.

Besides the role of the applied laser treatment to enhance electrical conductivity, these results can be related to the morphology of the Ag-PL composites (Figure 6; Figures S1–S3, Supporting

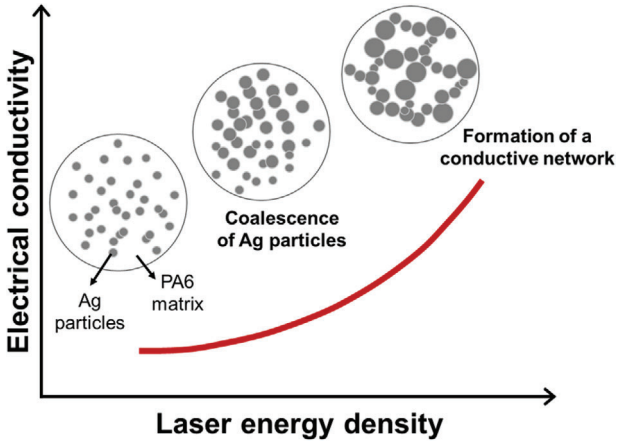

Figure 10. Effect of laser energy density on the electrical properties of the Ag-PL composites.

Information). It can be verified that the nanometric size of the Ag particles and their homogeneous distribution within the PA6 matrix contribute significantly to the conducting mechanism. Further, the established contacts between the Ag particle lead to tunable conductive properties.

Figure 10 summarizes the effect of the energy density of laser ablation technology on the electrical properties of the Ag-PL composites. As confirmed by the results obtained, by laser ablation technology it is possible to transform a thermoplastic composite with resistive properties into a material with selected conductive paths by using a low-cost and lower environmental technique, that is, the laser ablation. Thus, by increasing the energy density, the Ag particles are exposed and based on a phenomenon of coalescence of the metal particles, a conductive network is established, allowing the current transfer across the polymer matrix.

4. Conclusions

A method to produce Ag-containing PA6 composites with electrical conductivity in selected zones activated by scanning laser treatment is presented. Through a one-step in situ polymerization process, MP loaded with Ag particles were synthesized. Then, molded composites were produced from the Ag-loaded MP by CM. The combination of a reactive method with a conventional CM process led to the production of composites with good homogenization of the metal filler and with no functionalization needed. Improvement of the thermal stability of the polymer matrix in the presence of the Ag particles was achieved, indicating the possibility to machine the composites by laser scanning treatment. The laser scanning treatment was utilized as the goal of this work was to produce selectively conductive paths in insulating composites rather than to transform the whole composite into a conductor. To create these conductive paths, it was employed an Nd: YAG laser irradiating selected parts of the Ag-PA6 composite plates. Thus, it was possible to induce electrical conductivity in specific parts of a thermoplastic composite with resistive properties by using a low-cost and lower environmental impact technique, that is, laser ablation. For the laser scanning conditions studied, electric conductivity values in the range of 1.12 to 8.90 S m^{-1} were measured in the laser-ablated line patterns. This means that the Ag particles promote charge mobility on the ablated surface, creating a conductive network. The effect of laser parameters was evaluated to find a relation between the exposed Ag particles, the electric conductive properties, and the aesthetic aspects of the composites. Thus, it was found a suitable compromise between these features at lower energy densities.

It should be noted that the concept of this study that combines the microencapsulation strategy for the preparation of thermoplastic composites followed by selective laser ablation to create conductive patterns can be applied not only with Ag but with other metal particles, that is, with ferromagnetic properties. This could increase the spectrum of applications of these advanced materials merging electrical conductivity and magnetic properties. In this sense, applications of Ag-loaded PA6 composites can be considered by patterning electroconductive networks wherever it is desirable.

Supporting Information

Supporting Information is available from the Wiley Online Library or from the author.

Acknowledgements

F.M.O., N.D., and Z.D. acknowledge the financial support by National Funds through Fundação para a Ciência e Tecnologia (FCT), project UID/CTM/50025/2019. N.D. is also grateful for the financial support of FCT in the frames of the personal program contract CTTI-51/18-IPC. F.M.O. would also like to the FCT for the Ph.D. grant PD/BD/114372/2016 (AdvaMTech—Ph.D. Program in Advanced Materials and Processing). C.G.M., O.C., and F.S.S. acknowledge the financial support by FCT in the scope of the projects UID/EEA/04436/2019 and Add.Additive_Manufacturing to Portuguese Industry_POCI-01-0247-FEDER-024533. C.G.M. also acknowledges CNPq (Ph.D. grant number: 205791/2014-0) for the financial support. The authors thank C. Jellett for his careful reading of this manuscript and useful comments.

Conflict of Interest

The authors declare no conflict of interest.

Data Availability Statement

Data sharing is not applicable to this article as no new data were created or analyzed in this study.

Keywords

anionic ring-opening polymerization, electrical conductivity, laser ablation, polyamide composites, silver nanoparticles

Received: May 3, 2021
Revised: June 22, 2021
Published online: July 16, 2021

[1] C. Yu, Y. S. Kim, D. Kim, J. C. Grunlan, *Nano Lett.* **2008**, *8*, 4428.

[2] H. Pang, L. Xu, D.-X. Yan, Z.-M. Li, *Prog. Polym. Sci.* **2014**, *39*, 1908.
[3] H. Zhao, R. Hu, P. Li, A. Gao, X. Sun, X. Zhang, X. Qi, Q. Fan, Y. Liu, X. Liu, M. Tian, G. Tao, L. Qu, *Nano Energy* **2020**, *76*, 104926.
[4] Y. P. Mamunya, V. V. Davydenko, P. Pissis, E. V. Lebedev, *Eur. Polym. J.* **2002**, *38*, 1887.
[5] A. Boudenne, L. Ibos, M. Fois, J. C. Majesté, E. Géhin, *Composites, Part A* **2005**, *36*, 1545.
[6] R. M. Bagwell, J. M. McManaman, R. C. Wetherhold, *Compos. Sci. Technol.* **2006**, *66*, 522.
[7] A. Al-Sayyad, J. Bardon, P. Hirchenhahn, K. Santos, L. Houssiau, P. Plapper, *Proc. CIRP* **2018**, *74*, 495.
[8] S.-G. Kim, A. Suzuki, N. Takata, M. Kobashi, *J. Mater. Process. Technol.* **2019**, *270*, 1.
[9] Y. Liang, X. Xia, Y. Luo, Z. Jia, *Mater. Lett.* **2007**, *61*, 3269.
[10] H. M. Song, Y. J. Kim, J. H. Park, *J. Phys. Chem. C* **2008**, *112*, 5397.
[11] A. Laachachi, M. Cochez, M. Ferriol, J. M. Lopez-Cuesta, E. Leroy, *Mater. Lett.* **2005**, *59*, 36.
[12] N. Patra, M. Salerno, M. Malerba, P. D. Cozzoli, A. Athanassiou, *Polym. Degrad. Stab.* **2011**, *96*, 1377.
[13] X. Wu, S. Takeshita, K. Tadumi, W. Dong, S. Horiuchi, H. Niino, T. Furuya, S. Yoda, *Mater. Chem. Phys.* **2019**, *222*, 300.
[14] H. Althues, J. Henle, S. Kaskel, *Chem. Soc. Rev.* **2007**, *36*, 1454.
[15] H. Zhang, X. Zhong, J.-J. Xu, H.-Y. Chen, *Langmuir* **2008**, *24*, 13748.
[16] J. L. Zhang, R. S. Srivastava, R. D. K. Misra, *Langmuir* **2007**, *23*, 6342.
[17] E. M. Palmero, J. Rial, J. de Vicente, J. Camarero, B. Skårman, H. Vidarsson, P.-O. Larsson, A. Bollero, *Sci. Technol. Adv. Mater.* **2018**, *19*, 465.
[18] M. H. Al-Saleh, G. A. Gelves, U. Sundararaj, *Composites, Part A* **2011**, *42*, 92.
[19] A. M. Khalil, M. L. Hassan, A. A. Ward, *Carbohydr. Polym.* **2017**, *157*, 503.
[20] M. Jalali, S. Dauterstedt, A. Michaud, R. Wuthrich, *Composites, Part B* **2011**, *42*, 1420.
[21] T. Peter, M. Wegner, V. Zaporojtchenko, T. Strunskus, S. Bornholdt, H. Kersten, F. Faupel, *Surf. Coat. Technol.* **2011**, *205*, S38.
[22] G. Malandrino, *Angew. Chem., Int. Ed.* **2009**, *48*, 7478.
[23] R. Gonzalez, H. Ashrafizadeh, A. Lopera, P. Mertiny, A. McDonald, *J. Therm. Spray Technol.* **2016**, *25*, 897.
[24] P. Li, F. Yang, X. Li, C. He, W. Su, J. Chen, L. Huo, R. Chen, C. Lu, L. Liang, *Appl. Surf. Sci.* **2013**, *280*, 164.
[25] X. Wang, J. Liu, *Micromachines* **2016**, *7*, 206.
[26] C. Cano-Raya, Z. Z. Denchev, S. F. Cruz, J. C. Viana, *Appl. Mater. Today* **2019**, *15*, 416.
[27] H. Zhao, M. Tian, Z. Li, Y. Zhang, S. Zhu, X. Zhang, S. Chen, L. Qu, *Mater. Lett.* **2019**, *240*, 5.
[28] J. Šebenda, *J. Macromol. Sci., Part A: Chem.* **1972**, *6*, 1145.
[29] K. van Rijswijk, H. E. N. Bersee, *Composites, Part A* **2007**, *38*, 666.
[30] L. A. Utracki, *Polymer Blends Handbook*, Springer, Dordrecht, Netherlands **2014**.
[31] N. Dencheva, Z. Denchev, S. Lanceros-Méndez, T. E. Sanz, *Macromol. Mater. Eng.* **2016**, *301*, 119.
[32] C. Brêda, N. Dencheva, S. Lanceros-Mendez, Z. Denchev, *J. Mater. Sci.* **2016**, *51*, 10534.
[33] R. Zeng, M. Z. Rong, M. Q. Zhang, H. C. Liang, H. M. Zeng, *Appl. Surf. Sci.* **2002**, *187*, 239.
[34] L. D. Laude, S. Soudant, S. Beauvois, D. Renaut, A. Jadin, *Nucl. Instrum. Methods Phys. Res. B* **1997**, *131*, 211.
[35] K. C. A. Crane, J. R. Brown, *J. Phys. D: Appl. Phys.* **1981**, *14*, 2341.
[36] P. Rytlewski, *Electrochim. Acta* **2012**, *61*, 191.
[37] G. Rusu, K. Ueda, E. Rusu, M. Rusu, *Polymer* **2001**, *42*, 5669.
[38] G.-F. Shan, W. Yang, M. Yang, B. Xie, J. Feng, Q. Fu, *Polymer* **2007**, *48*, 2958.
[39] F. Dan, C. Vasiliu-Oprea, *Colloid Polym. Sci.* **1998**, *276*, 483.
[40] C. Vasiliu-Oprea, F. Dan, *J. Appl. Polym. Sci.* **1996**, *62*, 1517.
[41] L. Ricco, O. Monticelli, S. Russo, A. Paglianti, A. Mariani, *Macromol. Chem. Phys.* **2002**, *203*, 1436.
[42] T. D. Fornes, D. R. Paul, *Polymer* **2003**, *44*, 3945.
[43] Y. Li, W. A. Goddard, *Macromolecules* **2002**, *35*, 8440.
[44] A. Riveiro, A. L. B. Maçon, J. del Val, R. Comesaña, J. Pou, *Front. Phys.* **2018**, *6*, 16.
[45] T. Lippert, in *Polymers and Light* (Ed: T.K. Lippert), Springer, Berlin **2004**, pp. 51–246.
[46] H. V. Atkinson, S. Davies, *Metall. Mater. Trans. A* **2000**, *31*, 2981.
[47] G. Becherer, R. Ifland, *Naturwissenschaften* **1954**, *41*, 471.
[48] P. A. M. Steeman, J. van Turnhout, in *Broadband Dielectric Spectroscopy* (Eds: F. Kremer, A. Schönhals), Springer, Berlin **2003**, pp. 495–522.
[49] H. D. Young, Roger, *University Physics With Modern Physics* (Eds: H.D. Young, R.A. Freedman), Addison-Wesley, San Francisco **2012**, p. 823.
[50] R. Strümpler, J. Glatz-Reichenbach, *J. Electroceram.* **1999**, *3*, 329.

